materials proceedings

MDPI

Proceeding Paper

Enhanced Supercapacitor Performance through the Synergistic Effects of a Biomass-Derived Activated Carbon and Electrochemically Deposited Polyaniline Composite †

Syed Shaheen Shah [1,*], Md. Abdul Aziz [2,*] and Munetaka Oyama [1]

1 Department of Material Chemistry, Graduate School of Engineering, Kyoto University, Nishikyo-ku, Kyoto 615-8520, Japan; oyama.munetaka.4m@kyoto-u.ac.jp
2 Interdisciplinary Research Center for Hydrogen Technologies and Carbon Management (IRC-HTCM), King Fahd University of Petroleum & Minerals, KFUPM Box 5040, Dhahran 31261, Saudi Arabia
* Correspondence: shah.syedshaheen.78r@st.kyoto-u.ac.jp (S.S.S.); maziz@kfupm.edu.sa (M.A.A.)
† Presented at the 6th Conference on Emerging Materials and Processes (CEMP 2023), Islamabad, Pakistan, 22–23 November 2023.

Abstract: This research delves into asymmetric supercapacitor (ASC) design, utilizing activated carbon from bamboo poles (AC) and electrodeposited polyaniline (PANI) on nickel foam (NF) as key active components. The composite electrode formed from AC and PANI exhibited enhanced electrochemical attributes in various electrochemical configurations. The specified ASC, PANI@AC/NF//AC/NF, demonstrated a potential of 1.8 V. Impressively, it reached an areal capacitance measuring 423 mF/cm^2, coupled with an energy density of 190 μWh/cm^2 at a power density of 900 μW/cm^2, and maintained ~82% capacitance after 5000 GCD cycles. Notably, our developed ASC presents outstanding research potential for scholars and scientists.

Keywords: biomass-derived activated carbon; polyaniline; electrochemical deposition; composite electrodes; ionic liquid electrolyte; asymmetric supercapacitor

check for updates

Citation: Shah, S.S.; Aziz, M.A.; Oyama, M. Enhanced Supercapacitor Performance through the Synergistic Effects of a Biomass-Derived Activated Carbon and Electrochemically Deposited Polyaniline Composite. *Mater. Proc.* **2024**, *17*, 29. https://doi.org/10.3390/materproc2024017029

Academic Editors: Sofia Javed, Waheed Miran, Erum Pervaiz and Iftikhar Ahmad

Published: 24 April 2024

1. Introduction

Supercapacitors, merging the best of capacitors and batteries, are gaining prominence for their rapid charge-discharge and long operational cycles [1]. The efficiency of these devices hinges on electrode material selection, crucial for energy retention and overall performance [2]. This study focuses on activated carbon (AC), known for its high electrical conductivity and surface area [3], and polyaniline (PANI), recognized for its pseudocapacitive [4,5], redox-based capacitance enhancement [2,3]. We explore bamboo poles as a novel, sustainable source for AC, and investigate the synergistic potential of combining AC and PANI in supercapacitors. This research presents the fabrication and electrochemical characterization of an asymmetric supercapacitor (ASC), using bamboo-derived AC and PANI deposited on nickel foam. Our goal is to elucidate how this material combination can boost ASC performance, paving the way for future innovations in energy storage technology. The synergistic combination of biomass-derived carbon and PANI in ASC harnesses the high surface area and conductivity of carbon with the pseudocapacitive properties of PANI, significantly enhancing energy storage and efficiency. This innovative blend not only promises a leap in ASC performance, but also sets a sustainable pathway for future energy storage solutions.

2. Materials and Experimental Methods

2.1. Materials

1-butyl-3-methylimidazolium hexafluorophosphate (BMIMBF, ≥97.0%), Aniline monomer (≥99.5%), polyvinylidene fluoride (PVDF, M_w~534,000), sodium bicarbonate

($NaHCO_3$, ≥99.7%), N-methyl-2-pyrrolidone (NMP, 99.5%), potassium hydroxide (KOH, ≥85%), hydrochloric acid (HCl, 37%), and sulfuric acid (H_2SO_4, 99.999%) were all procured from Sigma Aldrich (St. Louis, MI, USA). Nickle foam (NF) was obtained from Amazon in Japan and bamboo poles were collected from Kyoto University, Japan.

2.2. Synthesis of Electrode Materials and Fabrication of ASC

AC was produced from bamboo poles through a simple pyrolytic process. After cleaning with de-ionized (DI) water and drying, the poles were ground and combined with $NaHCO_3$. This mixture underwent thermal treatment at 800 °C for 5 h in a N_2 environment. The resulting material was purified with HCl and DI water, and then dried at 80 °C to yield the final AC product. The AC/NF electrode was fabricated by blending 90 wt.% synthesized AC with 10 wt.% PVDF binder. After dissolving PVDF in NMP and integrating AC, a uniform slurry was cast onto NF and were subjected to drying at 70 °C for 12 h. PANI's electrochemical deposition on NF and AC/NF was optimized at +0.8 V vs. Ag/AgCl for 300 s, using a 0.5 M aniline in 1 M H_2SO_4 electrolytic solution. The PANI@AC/NF exhibited superior current density (Figure 1), indicating efficient deposition. As shown in Figure 1, the ASC was assembled with AC/NF as the negatrode and PANI@AC/NF as the positrode (PANI@AC/NF//AC/NF), using a BMIMBF electrolyte-saturated filter paper separator. Electrochemical assessments, i.e., galvanostatic charge–discharge (GCD), cyclic voltammetry (CV), and electrochemical impedance spectroscopy (EIS), were performed, with capacitance and energy/power densities measured from specific equations [6,7].

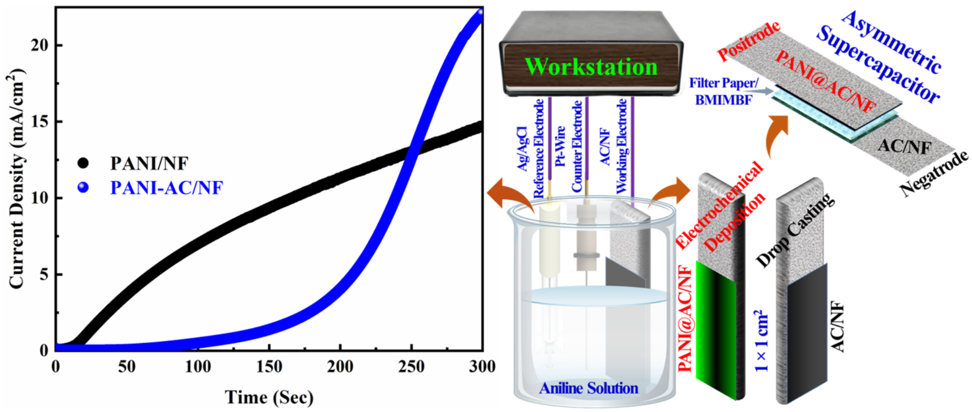

Figure 1. Amperometric response on a bare and AC-modified NF substrate and the corresponding PANI@AC/NF//AC/NF ASC.

3. Results and Discussion

The XRD technique was employed to elucidate the structural nuances of the PANI/NF, AC, and bare NF, as illustrated in Figure 2a. For the bare NF, prominent diffraction peaks at specific 2θ values were identified, corresponding to its crystalline nature [8]. On the other hand, the PANI/NF spectrum displayed additional peaks between 10° to 40°, signifying the successful deposition of PANI over the NF. This was further corroborated by distinct peaks that align with literature findings [9]. AC's XRD pattern in Figure 2a exhibited broad peaks, indicative of its predominantly amorphous structure with a hint of crystallinity [6]. FESEM micrographs, as shown in Figure 2b,c, highlighted AC's heterogeneous and porous morphology, attributed to the volatilization during pyrolysis. Figure 2d,e and Figure 2f,g presented the morphologies of bare NF and PANI/NF, respectively. The NF's inherent porous structure ensures a uniform PANI distribution, enhancing conductivity and stability. The PANI's cohesive integration with the NF substrate underscores its potential as a superior electrode for supercapacitor applications.

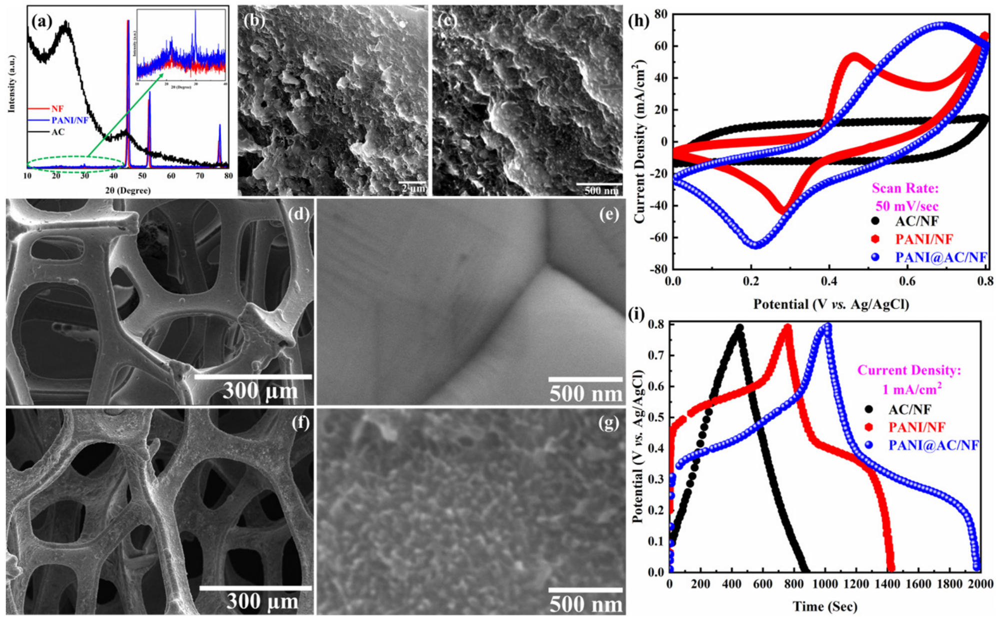

Figure 2. (**a**) XRD patterns and FESEM images of (**b**,**c**) AC, (**d**,**e**) NF, and (**f**,**g**) PANI/NF. (**h**) CV curves and (**i**) GCD profiles various prepared electrodes.

Figure 2h displays the CV curves recorded at a 5 mV/sec scan rate in 1 M KOH. AC/NF shows a quasi-rectangular pattern, with a 630 mF/cm^2 areal capacitance. PANI/NF, however, exhibits pronounced redox peaks, indicative of PANI's pseudocapacitive nature and an areal capacitance of 815 mF/cm^2. The composite PANI@AC/NF curve highlights a synergistic effect, achieving a peak areal capacitance of 1740 mF/cm^2. GCD analysis in Figure 2i reveals a similar approach with AC/NF's areal capacitance at 529 mF/cm^2, PANI/NF's at 833 mF/cm^2, and the composite's impressive 1180 mF/cm^2.

For the ASC configuration, the AC/NF was designated as the negatrode, while the PANI@AC/NF functioned as the positrode, culminating in the ASC represented as PANI@AC/NF//AC/NF. Figure 3a presents AC/NF and PANI@AC/NF CV curves recorded in their respective stable operating potential windows (OPWs). The AC/NF curve spans a negative 0 to −1 V OPW, while the PANI@AC/NF curve occupies a 0 to 0.8 V OPW. The combined theoretical OPW for the PANI@AC/NF//AC/NF ASC is approximately 1.8 V, indicating that the device's maximum operational voltage closely approaches this value. Figure 3b depicts the PANI@AC/NF//AC/NF ASC's CV curves across various scan rates within an OPW of 0 to 1.8 V. Notably, the curves exhibit a pronounced redox peak, characteristic of the PANI@AC/NF//AC/NF device, while the electric double-layer behavior of AC imparts a quasi-rectangular shape. As the scan rate escalates, the area beneath the CV curves expands, accompanied by a surge in current density. The areal capacitance derived from the CV curves ranged from 252 to 607 mF/cm^2 with decrease in the scan rate from 100 to 10 mV/sec. Figure 3c displays the GCD patterns of the PANI@AC/NF//AC/NF ASC across various current densities. As the current density fluctuated between 5 and 1 mA/cm^2, the areal capacitances varied from 164 mF/cm^2 to 423 mF/cm^2. Notably, the ASC reached its maximum energy density of 190 µWh/cm^2 when operating at a power density of 900 µW/cm^2, depicted in Figure 3d.

Such commendable outcomes underline the synergistic potential of PANI and AC in bolstering electrochemical performances. Post 5000 GCD cycles, the device retained ~82% of its initial capacitance, underscoring its robust cycling stability (Figure 3e). In Figure 3f, the EIS Nyquist plots for the PANI@AC/NF//AC/NF ASC, both before and after 5000 GCD cycles, are expertly illustrated, spanning frequencies from 1 Hz to 1 MHz. These plots reveal a semi-circular trajectory in the high-frequency range, indicative of a low charge-transfer resistance (R_{ct}) and fast ion diffusion into the electrodes, and a near-vertical line in the low-frequency domain, highlighting ideal capacitive behavior. Notably, the high-frequency intercept pinpoints the equivalent series resistance, encompassing combined electrode, electrolyte, and interface resistances. The R_{ct} values, 18 Ohm initially and decreasing to 16 Ohm post 5000 cycles, demonstrate the system's robustness. Significantly, the inset of Figure 3f enriches our understanding by including the equivalent circuit diagram, offering a comprehensive view of the electrical dynamics at play.

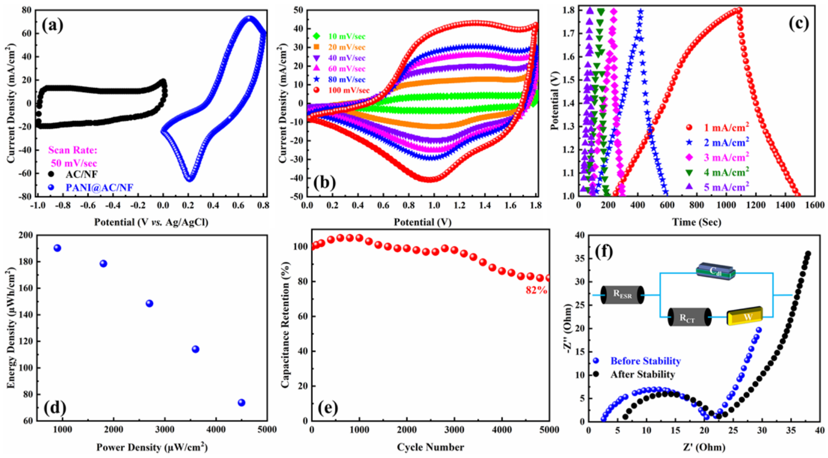

Figure 3. (**a**) CV curves of electrodes, (**b**) CV curves, (**c**) GCD profiles, (**d**) Ragon plot, (**e**) capacitance retention, and (**f**) Nyquist plots of the PANI@AC/NF//AC/NF ASC.

4. Conclusions

The research successfully demonstrated the potential of bamboo rod-derived AC and electrodeposited PANI in developing high-performance ASC. The meticulous synthesis and characterization processes ensured the purity and structural integrity of the materials. The synergistic effect between AC and PANI was prominently showcased in the PANI@AC/NF//AC/NF ASC, which achieved excellent electrochemical performance, including a maximum areal capacitance measuring 423 mF/cm^2, coupled with an energy density of 190 µWh/cm^2 at a power density of 900 µW/cm^2. Furthermore, its commendable cycling stability, retaining ~82% capacitance after 5000 cycles, underscores its potential for long-term applications. This research underscores the value of sustainable materials in energy storage, encouraging advancements through synergistic combinations.

Author Contributions: Conceptualization, S.S.S. and M.A.A.; methodology, S.S.S.; software, S.S.S.; validation, S.S.S., M.A.A. and M.O.; formal analysis, S.S.S.; investigation, S.S.S.; resources, S.S.S. and M.O.; data curation, S.S.S.; writing—original draft preparation, S.S.S.; writing—review and editing, S.S.S., M.A.A. and M.O.; visualization, S.S.S. and M.A.A.; supervision, M.O.; project administration, M.O.; funding acquisition, S.S.S. and M.O. All authors have read and agreed to the published version of the manuscript.

Funding: This research was funded by the Japan Society for the Promotion of Science under JSPS KAKENHI Grant 22F22336.

Institutional Review Board Statement: Not applicable.

Informed Consent Statement: Not applicable.

Data Availability Statement: Dataset available on request from the authors.

Acknowledgments: The authors thank the Japan Society for the Promotion of Science for their support and the postdoctoral fellowship for S. S. Shah.

Conflicts of Interest: The authors declare no conflicts of interest.

References

1. El-Kady, M.F.; Shao, Y.; Kaner, R.B. Graphene for batteries, supercapacitors and beyond. *Nat. Rev. Mater.* **2016**, *1*, 16033. [CrossRef]
2. Shah, S.S.; Oladepo, S.; Ali Ehsan, M.; Iali, W.; Alenaizan, A.; Nahid Siddiqui, M.; Oyama, M.; Al-Betar, A.-R.; Aziz, M.A. Recent Progress in Polyaniline and its Composites for Supercapacitors. *Chem. Rec.* **2023**, *24*, e202300105. [CrossRef] [PubMed]
3. Aziz, M.A.; Shah, S.S.; Mahnashi, Y.A.; Mahfoz, W.; Alzahrani, A.S.; Hakeem, A.S.; Shaikh, M.N. A High-Energy Asymmetric Supercapacitor Based on Tomato-Leaf-Derived Hierarchical Porous Activated Carbon and Electrochemically Deposited Polyaniline Electrodes for Battery-Free Heart-Pulse-Rate Monitoring. *Small* **2023**, *19*, 2300258. [CrossRef] [PubMed]
4. Yan, B.; Zheng, J.; Feng, L.; Zhang, Q.; Zhang, C.; Ding, Y.; Han, J.; Jiang, S.; He, S. Pore engineering: Structure-capacitance correlations for biomass-derived porous carbon materials. *Mater. Des.* **2023**, *229*, 111904. [CrossRef]
5. Demiral, H.; Demiral, İ. Surface properties of activated carbon prepared from wastes. *Surf. Interface Anal.* **2008**, *40*, 612–615. [CrossRef]
6. Shah, S.S.; Cevik, E.; Aziz, M.A.; Qahtan, T.F.; Bozkurt, A.; Yamani, Z.H. Jute Sticks Derived and Commercially Available Activated Carbons for Symmetric Supercapacitors with Bio-electrolyte: A Comparative Study. *Synth. Met.* **2021**, *277*, 116765. [CrossRef]
7. Shah, S.S.; Aziz, M.A.; Cevik, E.; Ali, M.; Gunday, S.T.; Bozkurt, A.; Yamani, Z.H. Sulfur nano-confinement in hierarchically porous jute derived activated carbon towards high-performance supercapacitor: Experimental and theoretical insights. *J. Energy Storage* **2022**, *56*, 105944. [CrossRef]
8. Shah, S.S.; Das, H.T.; Barai, H.R.; Aziz, M.A. Boosting the Electrochemical Performance of Polyaniline by One-Step Electrochemical Deposition on Nickel Foam for High-Performance Asymmetric Supercapacitor. *Polymers* **2022**, *14*, 270. [CrossRef] [PubMed]
9. Padmapriya, S.; Harinipriya, S.; Jaidev, K.; Sudha, V.; Kumar, D.; Pal, S. Storage and evolution of hydrogen in acidic medium by polyaniline. *Int. J. Energy Res.* **2018**, *42*, 1196–1209. [CrossRef]